

Sulfur Oxygenates of Biomimetics of the Diiron Subsite of the [FeFe]-Hydrogenase Active Site: Properties and Oxygen Damage Repair Possibilities

Tianbiao Liu, Bin Li, Michael L. Singleton, Michael B. Hall, and Marcetta Y. Darensbourg*

Department of Chemistry, Texas A&M University, College Station, Texas 77843

Received March 3, 2009; E-mail: marcetta@mail.chem.tamu.edu

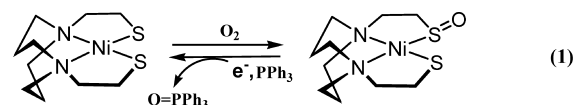
Abstract: This study explores the site specificity (sulfur vs the Fe–Fe bond) of oxygenation of diiron (Fe^IFe^I and Fe^{II}Fe^{II}) organometallics that model the 2-iron subsite in the active site of [FeFe]-hydrogenase: (μ -pdt)[Fe(CO)₂L][Fe(CO)₂L'] (L = L' = CO (**1**); L = PPh₃, L' = CO (**2**); L = L' = PMe₃ (**4**)) and (μ -pdt)(μ -H)[Fe(CO)₂PMe₃]₂ (**5**). DFT computations find that the Fe–Fe bond in the Fe^IFe^I diiron models is thermodynamically favored to produce the μ -oxo or oxidative addition product, Fe^{II}–O–Fe^{II}; nevertheless, the sulfur-based HOMO–1 accounts for the experimentally observed mono- and bis-O-atom adducts at sulfur, i.e., (μ -pst)[Fe(CO)₂L][Fe(CO)₂L'] (pst = –S(CH₂)₃S(O)–, 1,3-propanesulfenatothiolate; L = L' = CO (**1-O**); L = PPh₃, L' = CO (**2-O**); L = L' = PMe₃ (**4-O**)) and (μ -pds)[Fe(CO)₂L][Fe(CO)₂L'] (pds = –(O)S(CH₂)₃S(O)–, 1,3-propanedisulfenato; L = PPh₃, L' = CO (**2-O**₂)). The Fe^{II}(μ -H)Fe^{II} diiron model (**5**), for which the HOMO is largely of sulfur character, exclusively yields S-oxygenation. The depressing effect of such bridging ligand modification on the dynamic NMR properties arising from rotation of the Fe(CO)₃ correlates with higher barriers to the CO/PMe₃ exchange of (μ -pst)[Fe(CO)₃]₂ as compared to (μ -pdt)[Fe(CO)₃]₂. Five molecular structures are confirmed by X-ray diffraction: **1-O**, **2-O**, **2-O**₂, **4-O**, and **6**. Deoxygenation with reclamation of the μ -pdt parent complex occurs in a proton/electron-coupled process. The possible biological relevance of oxygenation and deoxygenation studies is discussed.

Introduction

The well-known oxygen sensitivity of hydrogenase (H₂ase) enzymes¹ and their active-site biomimetics poses a problem for their development as alternatives to platinum in fuel cell applications. As noted by Vincent et al., the deleterious effects of O₂ on the enzymes vary widely and are highly dependent on the type and source of the enzymes.² For example, the membrane-bound [NiFe]-H₂ase from *Ralstonia eutropha* is O₂ tolerant, while the [FeFe]-H₂ase from *Desulfovibrio desulfuricans* is irreversibly inactivated when exposed to O₂ in its H_{ox} state.² In its anaerobically overoxidized state, the O₂ damage may be reversed by reductive activation. Technological targets for synthetic biomimetic compounds^{3–9} and for genetically

modified enzymes¹⁰ lie in approaches to minimize or circumvent O₂ reactivity at the active metal catalyst site.

We have had interest in the ability of sulfur to act as a potential moderator of O₂ reactivity via formation of sulfoxo species such as metallosulfonates and metallosulfenates.¹¹ Studies of *cis*-dithiolato complexes of nickel, NiN₂S₂, established O-atom capture by thiolate sulfurs that modified the redox activity of the complexes but did not alter the Ni–S connectivity. In one case, reclamation of the thiolate was demonstrated to be possible by electrochemical reduction in the presence of an O-atom acceptor, eq 1.¹²



Such a process is possibly related to repair of oxygen-damaged [NiFe]-H₂ase, which has found myriad levels of activity recovery from oxidation.^{13–15} The nickel in [NiFe]H₂ase is surrounded

- (1) Adams, M. W. W. *Biochim. Biophys. Acta* **1990**, *1020*, 115–145.
- (2) Vincent, K. A.; Parkin, A.; Lenz, O.; Albracht, S. P. J.; Fontecilla-Camps, J. C.; Cammack, R.; Friedrich, B.; Armstrong, F. A. *J. Am. Chem. Soc.* **2005**, *127*, 18179–18189.
- (3) Darensbourg, M. Y.; Lyon, E. J.; Smece, J. J. *Coord. Chem. Rev.* **2000**, *206*, 533–561.
- (4) Liu, X. M.; Ibrahim, S. K.; Tard, C.; Pickett, C. J. *Coord. Chem. Rev.* **2005**, *249*, 1641–1652.
- (5) Sun, L. C.; Akermark, B.; Ott, S. *Coord. Chem. Rev.* **2005**, *249*, 1653–1663.
- (6) Song, L. C. *Acc. Chem. Res.* **2005**, *38*, 21–28.
- (7) Siegbahn, P. E. M.; Tye, J. W.; Hall, M. B. *Chem. Rev.* **2007**, *107*, 4414–4435.
- (8) Capon, J. F.; Gloaguen, F.; Petillon, F. Y.; Schollhammer, P.; Talarmin, J. *Eur. J. Inorg. Chem.* **2008**, 4671–4681.
- (9) Gloaguen, F.; Rauchfuss, T. B. *Chem. Soc. Rev.* **2009**, *38*, 100–108.

- (10) Ghirardi, M. L.; King, P. W.; Posewitz, M. C.; Maness, P. C.; Fedorov, A.; Kim, K.; Cohen, J.; Schulten, K.; Seibert, M. *Biochem. Soc. Trans.* **2005**, *33*, 70–72.
- (11) Grapperhaus, C. A.; Darensbourg, M. Y. *Acc. Chem. Res.* **1998**, *31*, 451–459.
- (12) Farmer, P. J.; Verpeaux, J. N.; Amatore, C.; Darensbourg, M. Y.; Musie, G. *J. Am. Chem. Soc.* **1994**, *116*, 9355–9356.
- (13) Seefeldt, L. C.; Arp, D. J. *Biochemistry* **1989**, *28*, 1588–1596.
- (14) Vanderzwaan, J. W.; Coremans, J.; Bouwens, E. C. M.; Albracht, S. P. J. *Biochim. Biophys. Acta* **1990**, *1041*, 101–110.

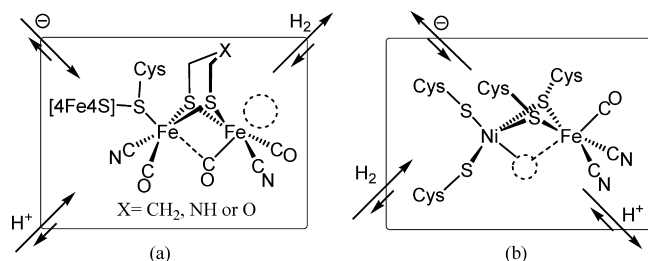


Figure 1. Sketches of [NiFe]- and [FeFe]-H₂ase active sites.

by cysteine S-donors, two of which serve as bridges to an adjacent Fe(CO)(CN)₂, and two of which are directed toward a hydrophobic channel within the protein, presumed to provide access or egress of diatomics, such as H₂ or unwanted, adventitious O₂ molecules, Figure 1.¹⁶ An attractive hypothesis is that the temporary formation of sulfoxo species might preserve enzyme active-site integrity following moderate exposure to O₂ and be more easily repaired than metal oxide formation.¹²

The two-iron subsite in the active site of [FeFe]-H₂ase is sketched in Figure 1: it contains three thiolate S-donors, two of which serve as a bidentate bridging ligand to the two irons.¹⁶ A popular precursor to biomimetics of this site is (μ-S(CH₂)₃S)[Fe^I(CO)₃]₂ or (μ-pdt)[Fe^I(CO)₃]₂.¹⁷ Modifications by CO ligand substitution with better donor ligands L are known to enhance reactivity toward electrophiles such as H⁺,^{18–21} RS⁺,²² and R⁺.²³ In the case of (μ-pdt)[Fe^I(CO)₂PMe₃]₂, H⁺ and RS⁺ attack the Fe–Fe bond density, generating oxidative addition products [(μ-E)(μ-pdt)[Fe^{II}(CO)₂L]₂⁺ with bridging E[–] groups.^{22,23} The R⁺ electrophile attacks the bridging thiolate sulfur, yielding a stable [(μ-edt-R)[Fe^I(CO)₂L]₂⁺,²³ Scheme 1. As suggested from computational studies, the better covalent bond between S and C accounts for the regioselectivity of alkylation, while iron-based protonation, generating the bridging hydride, yields a product some 30 kcal/mol more stable than the product of S-based protonation, generating a bridging thiol.²⁴

Since μ-oxo iron derivatives are well known,^{25,26} we questioned whether O-atom addition to (μ-pdt)[Fe^I(CO)₂L]₂ might provide examples of both S-site and metal-site reactivity. These studies are described herein. A sulfur-based O-atom adduct of the μ-1,2-ethanesulfenatothiolate (μ-est) complex, [(μ-est)[Fe^I(CO)₃]₂, similar to those described below was reported by

Messelhäuser et al. in 1987,²⁷ and during our manuscript preparation, Weigand et al. published complexes in the same class.²⁸ To our knowledge, those are the rare descriptions of sulfoxo species of organoiron compounds prior to our study.

Experimental Section

Materials and Techniques. All reactions and operations were conducted on a double-manifold Schlenk vacuum line under N₂ or Ar atmosphere. Hexane, tetrahydrofuran (THF), CH₂Cl₂, CH₃CN, and toluene were first degassed with N₂ for 30 min and then purified by an MBraun Manual Solvent Purification System packed with Alcoa F200 activated alumina desiccant. Hexane and toluene were freshly collected from the solvent system and used in experiments. The purified THF, CH₂Cl₂, and CH₃CN were stored over molecular sieves under N₂ for 24 h prior to further purification: THF was distilled under N₂ from sodium/benzophenone; CH₂Cl₂, CaCl₂, and CH₃CN were first stirred with CaH₂ at 22 °C for 5 h and then distilled. The collected CH₂Cl₂ and CH₃CN were stored over molecular sieves under Ar for experimental uses.

The complexes (μ-pdt)[Fe(CO)₃]₂,²⁹ (μ-pdt)[Fe(CO)₂PMe₃]₂,¹⁹ (μ-pdt)(μ-H)[Fe(CO)₂PMe₃]₂⁺PF₆[–],¹⁹ (μ-pdt)[Fe(CO)₃][Fe(CO)₂PPh₃]₂ (pdt = 1,3-propanedithiolate),³⁰ and dimethyldioxirane (DDO)³¹ were prepared according to published procedures. The following materials were of reagent grade and were directly used as purchased from Sigma-Aldrich or TCI Chemical Co.: *m*-chloroperoxybenzoic acid (*m*-CPBA), H₂O₂, Fe₃(CO)₁₂, FcPF₆, and Cp*₂Co.

¹H and ³¹P NMR spectra were measured on a Unity+ 300 MHz superconducting NMR instrument. Variable-temperature ¹³C NMR spectra were collected on natural abundance samples using a Unity+ 500 MHz superconducting NMR instrument operating at 125.9 MHz. Solution infrared spectra were measured on a Bruker Tensor 27 FTIR spectrometer using 0.1 mm NaCl sealed cells.

X-ray Structure Determinations. For all reported structures, a Bausch and Lomb 10× microscope was used to identify suitable crystals of the same habit. Each crystal was coated in paratone, affixed to a Nylon loop, and placed under streaming nitrogen (110 K) in a Bruker SMART 1000 CCD or Bruker-D8 Adv GADDS diffractometer (see details in CIF files in the Supporting Information). The space groups were determined on the basis of systematic absences and intensity statistics. The structures were solved by direct methods and refined by full-matrix least-squares on F². Anisotropic displacement parameters were determined for all non-hydrogen atoms. Hydrogen atoms were placed at idealized positions and refined with fixed isotropic displacement parameters. The following is a list of programs used: data collection and cell refinement, SMART WNT/2000 Version 5.632³² or FRAMBO³³ Version 4.1.05 (GADDS); data reductions, SAINTPLUS Version 6.63,³⁴ absorption correction, SADABS,³⁵ structural solutions, SHELXS-97;³⁶ struc-

(15) Coremans, J.; Vanderzwaan, J. W.; Albracht, S. P. J. *Biochim. Biophys. Acta* **1992**, *1119*, 157–168.

(16) Fontecilla-Camps, J. C.; Volbeda, A.; Cavazza, C.; Nicolet, Y. *Chem. Rev.* **2007**, *107*, 4273–4303.

(17) Seyferth, D.; Womack, G. B.; Gallagher, M. K.; Cowie, M.; Hames, B. W.; Fackler, J. P.; Mazany, A. M. *Organometallics* **1987**, *6*, 283–294.

(18) Dong, W. B.; Wang, M.; Liu, T. B.; Liu, X. Y.; Jin, K.; Sun, L. C. *J. Inorg. Biochem.* **2007**, *101*, 506–513.

(19) Zhao, X.; Georgakaki, I. P.; Miller, M. L.; Yarbrough, J. C.; Darensbourg, M. Y. *J. Am. Chem. Soc.* **2001**, *123*, 9710–9711.

(20) Ezzaher, S.; Capon, J. F.; Gloaguen, F.; Petillon, F. Y.; Schollhammer, P.; Talarmin, J. *Inorg. Chem.* **2007**, *46*, 3426–3428.

(21) Barton, B. E.; Rauchfuss, T. B. *Inorg. Chem.* **2008**, *47*, 2261–2263.

(22) Georgakaki, I. P.; Miller, M. L.; Darensbourg, M. Y. *Inorg. Chem.* **2003**, *42*, 2489–2494.

(23) Zhao, X.; Georgakaki, I. P.; Miller, M. L.; Mejia-Rodriguez, R.; Chiang, C. Y.; Darensbourg, M. Y. *Inorg. Chem.* **2002**, *41*, 3917–3928.

(24) Tye, J. W.; Darensbourg, M. Y.; Hall, M. B. *Theochem-J. Mol. Struct.* **2006**, *771*, 123–128.

(25) Kurtz, D. M. *Chem. Rev.* **1990**, *90*, 585–606.

(26) Tshuva, E. Y.; Lippard, S. J. *Chem. Rev.* **2004**, *104*, 987–1012.

(27) Messelhäuser, J.; Gutensohn, K. U.; Lorenz, I.-P.; Hiller, W. *J. Organomet. Chem.* **1987**, *321*, 377–388.

(28) Windhager, J.; Seidel, R. A.; Apfel, U. P.; Goerls, H.; Linti, G.; Weigand, W. *Chem. Biodiversity* **2008**, *5*, 2023–2041.

(29) Lyon, E. J.; Georgakaki, I. P.; Reibenspies, J. H.; Darensbourg, M. Y. *J. Am. Chem. Soc.* **2001**, *123*, 3268–3278.

(30) Li, P.; Wang, M.; He, C. J.; Li, G. H.; Liu, X. Y.; Chen, C. N.; Akermark, B.; Sun, L. C. *Eur. J. Inorg. Chem.* **2005**, 2506–2513.

(31) Murray, R. W.; Jeyaraman, R. *J. Org. Chem.* **1985**, *50*, 2847–2853.

(32) SMART V5.632 Program for Data Collection on Area Detectors; Bruker AXS Inc.: Madison, WI.

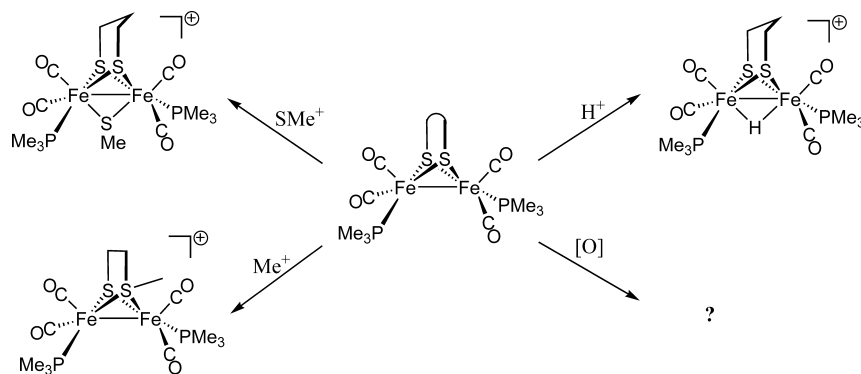
(33) FRAMBO:FRAME Buffer Operation Version 41.05 Program for Data Collection on Area Detectors; Bruker AXS Inc.: Madison, WI.

(34) SAINT V6.63 Program for Reduction of Area Detector Data; Bruker AXS Inc.: Madison, WI.

(35) Shelldrick, G. M. SADABS Program for Absorption Correction of Area Detector Frames; Bruker AXS.: Madison, WI.

(36) Shelldrick, G. SHELXS-97 Program for Crystal Structure Solution; Institut für Anorganische Chemie der Universität Göttingen: Göttingen, Germany, 1997.

Scheme 1



tural refinement, SHELXL-97,³⁷ graphics and publication materials, X-Seed Version 1.5.³⁸

Electrochemistry. Measurements were carried out using a BAS 100A electrochemical analyzer. All voltammograms were obtained in a conventional and gastight three-electrode cell under Ar atmosphere at 22 °C. The working electrode was a glassy carbon disk (0.071 cm²) which was successively polished with 15-, 3-, and 1- μ m diamond paste three times and alternately cleaned with deionized water after each polish treatment. The electrode was then sonicated in MeOH for 15 min prior to use. The supporting electrolyte was 0.1 M *n*-Bu₄NBF₄ in CH₃CN. The experimental reference electrode was Ag/Ag⁺, prepared by anodizing a silver wire in a CH₃CN solution of 0.01 M AgNO₃/0.1 M *n*-Bu₄NBF₄. The counter electrode was a platinum wire. All potentials were measured in CH₃CN solutions which were 0.1 M in *n*-Bu₄NBF₄, and reported relative to Fc⁺/Fc as an internal standard.

Theoretical Details. DFT calculations were performed using a hybrid functional [the three-parameter exchange functional of Becke (B3)³⁹ and the correlation functional of Lee, Yang, and Parr (LYP)⁴⁰ (B3LYP) as implemented in Gaussian 03⁴¹]. The effective core potentials and associated basis set of Hay and Wadt (LANL2DZ)^{42,43} were used on the iron, sulfur, and phosphorus atoms. For iron, the two outermost p functions were replaced by the reoptimized 4p functions as suggest by Couty and Hall.⁴⁴ For sulfur and phosphorus, the basis set was augmented by the d polarization function of Höllwarth et al.⁴⁵ All carbon, oxygen, and hydrogen atoms were represented using Dunning's double- ζ valence basis (D95)^{46,47} or Dunning's correlation-consistent polarized valence double- ζ basis set (cc-pVDZ).⁴⁸ Reported in the text are results from the former, while a complete table containing results from both basis sets is given in the Supporting Information (Table S2). The total free energies of oxygenate isomers **1-O** and **1- μ -O** from complex **1** were also compared by calculations using the TPSS⁴⁹ functional with the basis sets of LANL2DZ and cc-pVDZ. The geometries of all

Table 1. Infrared Spectroscopic Data, $\nu(\text{CO})$ Region, for Sulfur-Oxygenated Complexes (**1-O**, **2-O**, **2-O₂**, **4-O**, **5-O**, and **6**) in CH₂Cl₂, and Their Corresponding Precursors in Solvents as Listed

complex	$\nu(\text{CO})$ (cm ⁻¹)
(μ -pdt)[Fe(CO) ₃] ₂ (1)	2073 (m), 2035 (vs), 1992 (s, br) (CH ₃ CN)
(μ -pdt)[Fe(CO) ₃][Fe(CO) ₂ PPh ₃] (2)	2044 (s), 1982 (vs, br), 1931 (w) (CH ₃ CN)
(μ -pdt)[Fe(CO) ₂ PMe ₃] ₂ (4)	1979 (w), 1942 (s), 1898 (s) (CH ₃ CN)
(μ -pdt)(μ -H)[Fe(CO) ₂ PMe ₃] ₂ (5)	2048 (w, sh), 2033 (s), 1990 (s) (CH ₂ Cl ₂)
(μ -pst)[Fe(CO) ₃] ₂ (1-O)	2083 (m), 2045 (vs), 2017 (s), 2000 (s)
(μ -pst)[Fe(CO) ₃][Fe(CO) ₂ PPh ₃] (2-O)	2056 (s), 1998 (vs), 1971 (w), 1953 (w)
(μ -pds)[Fe(CO) ₃][Fe(CO) ₂ PPh ₃] (2-O₂)	2066 (s), 2014 (vs), 1981 (m), 1952 (w)
(μ -pst)[Fe(CO) ₂ PMe ₃] ₂ (4-O)	1994 (w), 1985 (w), 1958 (vs), 1917 (br, m)
(μ -pst)[Fe(CO) ₂ PMe ₃] ₂ (5-O)	2061 (w, sh), 2044 (s), 2002 (s)
Fe(CO) ₂ (PMe ₃) ₂ (<i>m</i> -Cl-PhCOO ⁻) ₂ (6)	2033 (s), 1981 (s)

oxygenate isomers and non-oxygenate precursors were fully optimized and confirmed as minima by analytical frequency calculations at the same levels.

Synthesis of (μ -pst)[Fe(CO)₃]₂ (1-O**).** Method A: Complex **1-O** was synthesized by slightly modifying the reported procedure for (μ -est)[Fe(CO)₃]₂.²⁷ To a toluene solution of complex **1** (1.00 g, 2.59 mmol in 50 mL) was added dropwise 1.5 equiv of oxidant, *m*-CPBA dissolved in 50 mL of toluene. The mixture was stirred for 0.5 h at 22 °C. Subsequently, the reaction solution was bubbled with ammonia gas for 20 min to remove excess *m*-CPBA and the *m*-chlorobenzoic acid byproduct. After filtration and *in vacuo* removal of toluene, the crude product (0.99 g, 95% yield) was dissolved in a minimum of MeOH and crystallized at -30 °C to give analytically pure product (0.87 g, 84% yield). Crystals suitable for X-ray analysis were grown from CH₂Cl₂ solution layered with hexane. IR: $\nu(\text{CO})$ data are given in Table 1 for a comprehensive comparison with other complexes (*vide infra*). ¹H NMR (ppm, acetone-*d*₆): 3.6 (t, 2H, -S(O)CH₂), 2.3 (p, 2H, -CH₂CH₂CH₂-), 2.1 (t, 2H, -CH₂CH₂S-). MS (ESI): *m/z* 402.82 [M + H⁺]. Elemental analysis: found (calcd) C, 26.89 (26.93); H, 1.50 (1.50).

Method B: To an acetone solution of complex **1** (0.20 g, 0.52 mmol in 20 mL) was added dropwise 20 mL of DDO acetone solution (ca. 0.05 mM). The mixture was stirred for 10 min at 22 °C to reach completion as indicated by IR monitor. After removal of solvent, the product was obtained in a yield of 92%, 192 mg.

Synthesis of (μ -pst)[Fe(CO)₃][Fe(CO)₂PPh₃] (2-O**).** Method A: The procedure used to synthesize complex **1-O** was applied to prepare complex **2-O** from complex **2** (1.00 g, 1.61 mmol) to provide crude product (93%). Further purification was achieved by

(37) Sheldrick, G. *SHELXL-97 Program for Crystal Structure Refinement*; Institut für Anorganische Chemie der Universität Göttingen: Göttingen, Germany, 1997.

(38) Barbour, L. J. *J. Supramol. Chem.* **2001**, *1*, 189–191.

(39) Becke, A. D. *J. Chem. Phys.* **1993**, *98*, 5648–5652.

(40) Lee, C.; Yang, W.; Parr, R. G. *Phys. Rev. B: Condens. Matter* **1988**, *37*, 785.

(41) Frisch, M. J.; et al. *Gaussian 03, Revision B.04*; Gaussian, Inc.: Wallingford, CT, 2004.

(42) Hay, P. J.; Wadt, W. R. *J. Chem. Phys.* **1985**, *82*, 270–283.

(43) Wadt, W. R.; Hay, P. J. *J. Chem. Phys.* **1985**, *82*, 284–298.

(44) Couty, M.; Hall, M. B. *J. Comput. Chem.* **1996**, *17*, 1359–1370.

(45) Höllwarth, A.; Böhme, M.; Dapprich, S.; Ehlers, A. W.; Gobbi, A.; Jonas, V.; Köhler, K. F.; Stegmann, R.; Veldkamp, A.; Frenking, G. *Chem. Phys. Lett.* **1993**, *208*, 237–240.

(46) Dunning, J. T. H. *J. Chem. Phys.* **1970**, *53*, 2823–2833.

(47) Dunning, J. T. H.; Hay, P. J. In *Methods of Electronic Structure Theory*; Schaefer, H. F., III., Ed.; Plenum Press: New York 1977, *3*.

(48) Dunning, J. T. H. *J. Chem. Phys.* **1989**, *90*, 1007–1023.

(49) Tao, J.; Perdew, J. P.; Staroverov, V. N.; Scuseria, G. E. *Phys. Rev. Lett.* **2003**, *91*, 146401.

precipitation from the saturated solution in CH₃CN at 0 °C. The final yield was 82% (0.84 g). Single crystals were grown from a solvent mixture of CH₂Cl₂ and pentane at –30 °C. Infrared data, $\nu(\text{CO})$ region, are given in Table 1. ¹H NMR (ppm, acetone-*d*₆): 7.74 (br, 6H, PPh₃), 7.63 (br, 9H, PPh₃), 3.23 (br 2H, –S(O)CH₂), 2.69 (br, 2H, –CH₂CH₂CH₂–), 1.95 (br, 2H, –CH₂CH₂S–). ³¹P NMR (ppm, acetone-*d*₆): 63.86. MS (ESI): *m/z* 636.91 [M + H⁺]. Elemental analysis: found (calcd) C, 48.83 (49.08); H, 3.40 (3.33).

Method B: An orange solution of **1-O** (0.50 g, 1.24 mmol) in 30 mL of CH₃CN was treated with an equal amount of Me₃NO (94 mg, 1.24 mmol) in 5 mL of CH₃CN. The solution color turned dark red, indicating formation of the intermediate ((μ -pst)[Fe(CO)₃][Fe(CO)₂NMe₃]) within 15 min as suggested by the IR monitor. To this solution was added 1 equiv of PPh₃ (0.327 g, 1.24 mmol) in 10 mL of CH₃CN, followed by heating at 80 °C for 5 h. After removal of volatiles under vacuum, the remaining red solids were washed with pentane (2 × 10 mL) and redissolved in CH₃CN. Pure product (0.67 g, 85%) precipitated from CH₃CN solution at –30 °C.

Synthesis of (μ -pds)[Fe(CO)₃][Fe(CO)₂PPh₃] (2-O₂**).** To complex **2-O** (0.50 g, 0.78 mmol) in 30 mL of toluene was added dropwise 1.5 equiv of *m*-CPBA in 30 mL of toluene. The solution was stirred at 22 °C for 0.5 h to convert all **2-O** as monitored by IR. The crude product (0.26 g, 50%) was obtained after treatment with NH₃ gas for 20 min and removal of solvent under vacuum. The crude product was then dissolved in 10 mL of hot MeOH and crystallized by cooling to 22 °C to give analytically pure product as orange needles (0.15 g, 29%). Crystals suitable for X-ray analysis were grown from CH₂Cl₂ solution layered with pentane. See Table 1 for $\nu(\text{CO})$ IR data. ¹H NMR (ppm, CH₂Cl₂-*d*₂): 7.65 (br, 6H, PPh₃), 7.55 (br, 9H, PPh₃), 3.42 (d, 4H, –S(O)CH₂), 3.14 (br, 2H, –CH₂CH₂CH₂–). ³¹P NMR (ppm, CH₂Cl₂-*d*₂): 64.4. MS (ESI): *m/z* 653.90 [M + H⁺]. Elemental analysis: found (calcd) C, 47.86 (47.88); H, 3.31 (3.25).

Synthesis of (μ -pst)[Fe(CO)₂PMe₃]₂ (4-O**).** Method A: An oily crude product of **4-O** was obtained from complex **4** (1.00 g, 2.07 mmol) by following the oxygenation procedure used to prepare complex **1-O**. Silica gel column chromatography with toluene eluent was performed under N₂. The red band was collected and concentrated to give a red residue. Over the course of a week, pure **4-O** precipitated from a –30 °C hexane solution in a yield of 83 mg (8%). Single crystals for X-ray analysis were grown from the saturated solution in CH₂Cl₂ at –30 °C. Infrared data, $\nu(\text{CO})$ region, are given in Table 1. ¹H NMR (ppm, CH₂Cl₂-*d*₂): 3.27 (br, 2H, –S(O)CH₂), 2.18 (br, 2H, –CH₂CH₂CH₂–), 1.76 (br, 2H, –CH₂CH₂S–), 1.53 (d, 18H, P(CH₃)₃). ³¹P NMR (ppm, CH₂Cl₂-*d*₂): 24.54. MS (ESI): *m/z* 498.93 [M + H⁺]. Elemental analysis: found (calcd) C, 30.88 (31.35); H, 4.83 (4.86).

Method B: Starting materials of complex **1-O** (1.00 g, 2.49 mmol) and excess PMe₃ (0.57 g, 8.07 mmol) were dissolved in 50 mL of toluene at 22 °C. The mixture was stirred at reflux temperature (110 °C) for 24 h, followed by filtration through a sintered glass frit to remove solid byproducts and subsequent evaporation of the filtrate to remove toluene. The resulting red product was subjected to silica gel column chromatography under N₂. Hexane was used as the first eluent to remove trace byproduct ((μ -pst)[Fe(CO)₃][Fe(CO)₂PMe₃] (**3**)). The second band was collected using toluene as eluent to give analytically pure complex **4-O** (0.77 g, 62%).

Isolation of Fe(CO)₂(PMe₃)₂(*m*-Cl-PhCOO[–])₂ (6**).** After the oxygenation of **4** and workup with ammonia gas as stated in method A to prepare **4-O**, solvent was removed under vacuum. The obtained residue was then extracted with 20 mL of hexane, followed by filtration through Celite. The hexane solution was slowly evaporated at 22 °C in 5 days to provide yellow-green crystals (**6**) at the top of the crystallization tube and red crystals (**4-O**) at the bottom. The crystals of **6** were manually chosen for X-ray and IR spectroscopic analyses. The $\nu(\text{CO})$ IR data are given in Table 1.

Synthesis of ((μ -pst)(μ -H)[Fe(CO)₂PMe₃]₂)⁺PF₆[–] (5-O**).** To complex **5** (0.50 g, 0.78 mmol) in 50 mL of CH₂Cl₂ was added dropwise 1.5 equiv of *m*-CPBA in 50 mL of CH₂Cl₂. The solution was stirred at 22 °C for 0.5 h to convert all **5** as monitored by IR. After removal of solvent, the remaining yellow solids were washed with ether (50 mL × 2) to remove excess oxidant and the *m*-chlorobenzoic acid byproduct. The crude product was dissolved in 10 mL of CH₂Cl₂ and then filtered through a sintered glass frit. The solution was layered with hexane, yielding the pure product as precipitate (0.36 g, 70%) at –30 °C in 3 days. IR $\nu(\text{CO})$ data are given in Table 1. ¹H NMR (ppm, CD₂Cl₂): 3.91 (br, 2H, –S(O)CH₂), 2.62 (br, 2H, –CH₂CH₂CH₂–), 2.4 (br, 2H, –CH₂CH₂S–), 1.66 (q, 18H, P(CH₃)₃), –13.33 (q, 1H, Fe₂H). ³¹P NMR (ppm, CH₂Cl₂-*d*₂), 25.8 (s, PMe₃), 149.2 (q, PF₆[–]). MS (ESI): *m/z* 498.93 [M – PF₆]⁺. Elemental analysis: found (calcd) C, 24.67 (24.24); H, 3.93 (3.91).

Deoxygenation of (μ -pst)[Fe(CO)₃]₂ (1-O**).** To a suspension of Cp*₂Co (0.33 g, 1 mmol) in a solvent mixture (10 mL, CH₃CN:H₂O, 50:1, v/v) was added dropwise complex **1-O** (0.2 g, 0.5 mmol) dissolved in the same solvent mixture (20 mL). The mixture was stirred at 22 °C for 30 min to reach completion as indicated by the IR monitor. Solvent was removed *in vacuo*, and solids obtained were extracted with 20 mL of hexane. The concentrated hexane solution was cooled at –30 °C to give complex **1** (96.5 mg, 50%). Complex **1** was further identified by ¹H NMR and FTIR spectroscopies.

Deoxygenation of (μ -pst)[Fe(CO)₃][Fe(CO)₂PPh₃] (2-O**) and (μ -pds)[Fe(CO)₃][Fe(CO)₂PPh₃] (**2-O₂**).** The procedure used to successfully deoxygenate complex **1-O** was applied to complexes **2-O** and **2-O₂**. Based on 0.20 g of starting material, complex **2** was isolated, 20 mg (10%) from **2-O** and 17 mg (9%) from **2-O₂**. The identity of complex **2** was confirmed by ¹H NMR and FTIR spectroscopies.

Deoxygenation of ((μ -pst)(μ -H)[Fe(CO)₂(PMe₃)₂]⁺PF₆[–] (5-O**).** The deoxygenation procedure as described for **1-O** was applied. A 0.27 g (0.04 mmol) sample of **5-O** was dissolved in the solvent mixture (5 mL, CH₃CN:H₂O = 50:1, v/v) and treated with 2 equiv of Cp*₂Co. The reaction was monitored by IR spectroscopy, indicating the generation of complexes **5** and **4-O**.

Electrochemical Deoxygenation of Sulfur-Oxygenated Complexes (1-O** and **4-O**).** Bulk electrolyses for electrochemical deoxygenation of sulfur-oxygenated complexes (**1-O** and **4-O**) were performed using a gastight 75 mL BASI bulk electrolysis cell equipped with four electrodes (Ag/Ag⁺ reference electrode, platinum counter electrode loaded in a fritted glass tube, glassy carbon working electrode, and a reticulated vitreous carbon (RVC) working electrode). During electrochemical experiments, the glassy carbon working electrode and RVC working electrode were switched between cyclic voltammetry (CV) and differential pulse voltammetry (DPV) and bulk electrolysis modes. Complex **1-O** (32 mg, 2 mmol), or **4-O** (40 mg, 2 mmol), was dissolved in 40 mL of electrolyte solution (CH₃CN:H₂O, 50:1, v/v, 0.1 M *n*-Bu₄NBF₄) in the cell. The first IR spectrum was measured before commencement of electrochemical experiments. The first CV and DPV were recorded using the glassy carbon working electrode. The RVC working electrode was then engaged to carry out bulk electrolysis at –1.7 V vs Fc⁺/Fc (2.3 V for complex **4-O**). After each equivalent of electrons passed through the RVC working electrode, the IR, CV, and DPV were measured to detect species present in the electrolyte solution. It was found that ca. 2 equiv of electrons was required to complete the electrochemical deoxygenation for complex **1-O**, while 3 equiv of electrons was needed for electrochemical deoxygenation of complex **4-O**.

Results and Discussion

Theoretical Predictions from DFT Computations. Prior to experimental oxygenation studies, DFT computations were carried out in an attempt to predict metal vs sulfur oxygenation

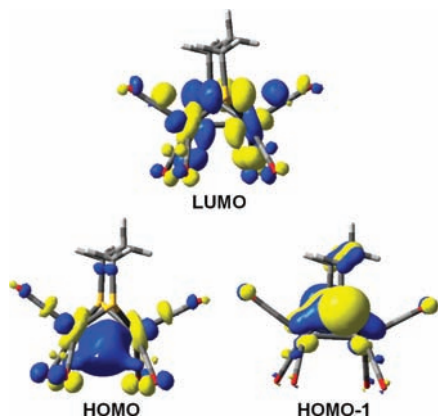


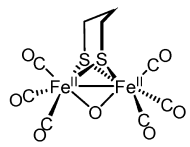
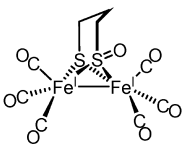
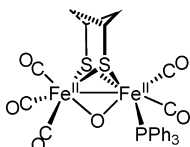
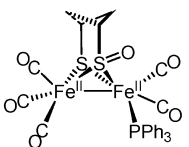
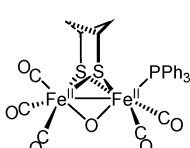
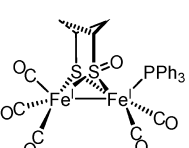
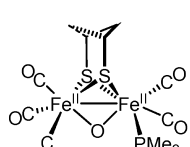
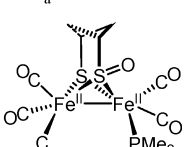
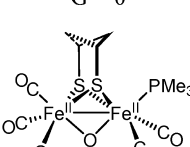
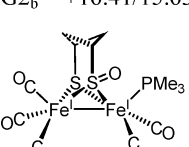
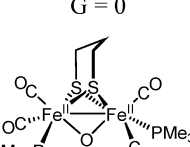
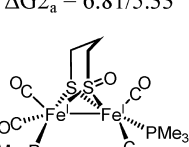
Figure 2. Frontier molecular orbitals (with isovalue = 0.04) of complex **1**, $(\mu\text{-pdt})[\text{Fe}(\text{CO})_3]_2$.

of the active-site paradigm of $[\text{FeFe}]\text{-H}_2\text{ase}$, $(\mu\text{-pdt})[\text{Fe}(\text{CO})_3]_2$ (**1**). Initially, geometry optimizations and vibrational frequency calculations were carried out on complex **1** and its oxygenated product isomers $(\mu\text{-pst})[\text{Fe}^{\text{I}}(\text{CO})_3]_2$ ($\mu\text{-pst} = \text{-SC}_3\text{H}_6\text{S}(\text{O})\text{-}$, propanesulfenatothiolate) (**1-O**) and $(\mu\text{-pdt})(\mu\text{-O})[\text{Fe}^{\text{II}}(\text{CO})_3]_2$ (**1- μ -O**) using the B3LYP functional with modified LANL2DZ basis sets for Fe and S and D95 basis sets for other atoms. The optimized structures of **1**, **1-O**, and **1- μ -O** were confirmed as energy minima by frequency calculations. The optimized structures of complexes **1** and **1-O** well match the metric data found experimentally by X-ray diffraction, which lends confidence to the correctness of the computation. Figure 2 displays the frontier molecular orbitals of **1**. As was earlier presented,⁵⁰ the HOMO is essentially the Fe–Fe bond density, while the HOMO–1 is characterized by the remaining lone pair on the bridging sulfur.

Table 2 lists total free energies of isomeric forms of **X-O** and **X- μ -O** (**X** = complexes **1–4**) obtained from the DFT calculations. For the all-CO complex **1**, the sulfur oxygenate is some 9.60 kcal/mol *less* stable than the diiron oxidative addition product, **1- μ -O**. As this is opposite the known experimental result of S-oxygenation determined for the $(\mu\text{-est})[\text{Fe}^{\text{I}}(\text{CO})_3]_2$ complex,²⁷ other basis sets were examined as a possible source of the discrepancy. When the computation was performed at the level of B3LYP/cc-PPVDZ&LANL2DZ (see Table S2), it was found that the total energy difference (ΔG_1) between **1-O** and **1- μ -O** is 10.76 kcal/mol, which is compatible with the result of 9.67 kcal/mol obtained from the initial calculation. In all cases, calculations at the level of B3LYP/cc-PPVDZ&LANL2DZ yielded slightly higher energies (see Table S2). Replacement of the B3LYP functional with TPSS led to the calculated value $\Delta G_1 = 11.66$ kcal/mol. Thus, qualitatively, the calculated ΔG_1 is not dependent on functionals or basis sets. From these data, theory predicts that the **1- μ -O** isomer is thermodynamically favored.

Similarly, in all cases, the $\mu\text{-O}$ isomeric form is calculated to be more stable for complexes **2- μ -O** vs **2-O**, **3- μ -O** vs **3-O**, and **4- μ -O** vs **4-O**. Again, as can be seen in Table S2, there is little difference in values determined from the two basis sets. Note that the positional isomers in complex **2**, i.e., PPh_3 in apical or basal positions, greatly affect the ΔG values (ΔG_{2a} vs ΔG_{2b}) of the isomeric oxygenates. Relative to the basal isomer, the S-oxygenate is favored when the phosphine is in the apical

Table 2. Total Free Energy (kcal/mol) Comparison between Sulfur-Oxygenated Species and Corresponding Metal-Oxygenated Isomers from the Computations with Functional and Basis Sets of B3LYP/D95&LANL2DZ

Isomeric oxygenates	
 1-μ-O $G = 0$	 1-O $\Delta G_1 = +9.60$
 2-μ-O-basal $G = 0$	 2-O-basal $\Delta G_{2b} = +16.70/17.00^a$
 2-μ-O-apical $G = 0$	 2-O-apical $\Delta G_{2a} = +5.90/4.40^a$
 3-μ-O-basal $G = 0$	 3-O-basal $\Delta G_{2b} = +16.41/15.63^a$
 3-μ-O-apical $G = 0$	 3-O-apical $\Delta G_{2a} = 6.81/5.33^a$
 4-μ-O $G = 0$	 4-O $\Delta G_4 = +19.50$

^a These selected values are for the structure with alternate direction of bridgehead carbon in the propane S-to-S linker (the dashed line).

position. For example, the total energy difference of **2- μ -O-basal** vs **2-O-basal** (ΔG_{2b}) is some 17 kcal/mol, while ΔG_{2a} is only ca. 5 kcal/mol, i.e., 10 kcal/mol less than the former. DFT computations at both levels suggest that the flip of the S–S linker has little effect (ca. 2 kcal/mol) on the total energy of the oxygenate isomers from **2**. For example, **2-O-apical** (5.90 kcal/mol) is 1.5 kcal/mol less stable than its S–S linker flipped

(50) Georgakaki, I. P.; Thomson, L. M.; Lyon, E. J.; Hall, M. B.; Darensbourg, M. Y. *Coord. Chem. Rev.* **2003**, *238*, 255–266.

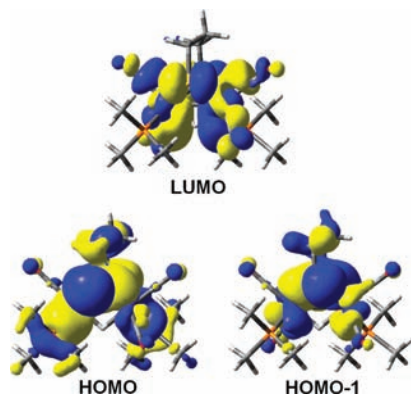


Figure 3. Frontier molecular orbitals (with isovalue = 0.04) of 5^+ , $\{(\mu\text{-pdt})(\mu\text{-H})[\text{Fe}(\text{CO})_2(\text{PMe}_3)_2]^+\}^+$.

isomer (4.40 kcal/mol, structure with the dashed line in Table 2). Ligand position and linker bridgehead position have similar effects on the total energy of the oxygenate isomers from **3**.

Figure 3 displays the frontier orbitals of the $\text{Fe}^{\text{II}}\text{Fe}^{\text{II}}$ complex, $\{(\mu\text{-pdt})(\mu\text{-H})[\text{Fe}(\text{CO})_2(\text{PMe}_3)_2]^+\}^+$ (5^+). Unlike the $\text{Fe}^{\text{I}}\text{Fe}^{\text{I}}$ species, the HOMO of complex 5^+ is largely the sulfur lone pair; i.e., addition of the proton into the Fe–Fe bond orbital greatly stabilizes what was the HOMO of complex **3**. Therefore, the orbital-directing oxygenation of 5^+ should be at sulfur.

Synthesis and Characterizations. Attempts to oxygenate $(\mu\text{-pdt})[\text{Fe}(\text{CO})_3]_2$ (**1**) (in acetonitrile and MeOH) with molecular O_2 resulted in slow precipitation of insoluble, non-CO-containing solids over the course of days without detection of any intermediate by IR spectroscopy. Complex **1** in acetone or acetonitrile was found to be inert toward H_2O_2 at 22 °C and at temperatures up to 80 °C. Therefore, we revisited the method used by Lorenz et al. to produce an oxygenate of $(\mu\text{-edt})[\text{Fe}(\text{CO})_3]_2$, i.e., $(\mu\text{-est})[\text{Fe}(\text{CO})_3]_2$, using *m*-CPBA as O-atom donor.²⁷ It was found out that the oxygenation of **1** by 1.5 equiv of *m*-CPBA in toluene proceeds smoothly within 0.5 h at 22 °C as indicated by the IR monitor, which showed on average a 10 cm^{-1} positive shift in $\nu(\text{CO})$ values. The reaction is accompanied by an obvious color change from red to golden yellow. Complex $(\mu\text{-pst})[\text{Fe}(\text{CO})_3]_2$ (**1-O**) was isolated as the sole product in 84% yield, and its identity was established by ESMS, IR, NMR, and X-ray diffraction. When an additional portion of oxidant was used after the formation of **1-O**, no new species was observed.

Similarly to *m*-CPBA, DDO oxygenates **1** to **1-O** in a quantitative yield. The advantage of using DDO over *m*-CPBA is the ease of purification of the oxygenated product since acetone is the only byproduct. The disadvantages lie in the low yield of DDO synthesis and its instability on storage.

The oxygenations of various $(\mu\text{-pdt})[\text{Fe}(\text{CO})_2\text{L}]_2$ were carried out as outlined in Scheme 2. Complex **2**, $(\mu\text{-pdt})[\text{Fe}(\text{CO})_3][\text{Fe}(\text{CO})_2\text{PPh}_3]$, behaves like complex **1** upon treatment with O_2 and H_2O_2 , but it readily reacts with 1.5 equiv of *m*-CPBA to give complex **2-O**, $(\mu\text{-pst})[\text{Fe}_2(\text{CO})_3][\text{Fe}_2(\text{CO})_2\text{PPh}_3]$ (82% yield). In contrast to complex **1-O**, on addition of another 1.5 equiv of *m*-CPBA, **2-O** undergoes further oxygenation at the remaining thiolate, as confirmed by various characterizations. Although the $\nu(\text{CO})$ IR monitor indicated a quantitative conversion, the isolated yield of $(\mu\text{-pds})[\text{Fe}(\text{CO})_3][\text{Fe}(\text{CO})_2\text{PPh}_3]$, **2-O₂** (pds = $-(\text{O})\text{S}(\text{CH}_2)_3\text{S}(\text{O})-$), is ca. 29% due to loss during purification.

The reactivity of complex **2** prompted study of the oxygenation of the more electron rich, and thus more air sensitive,

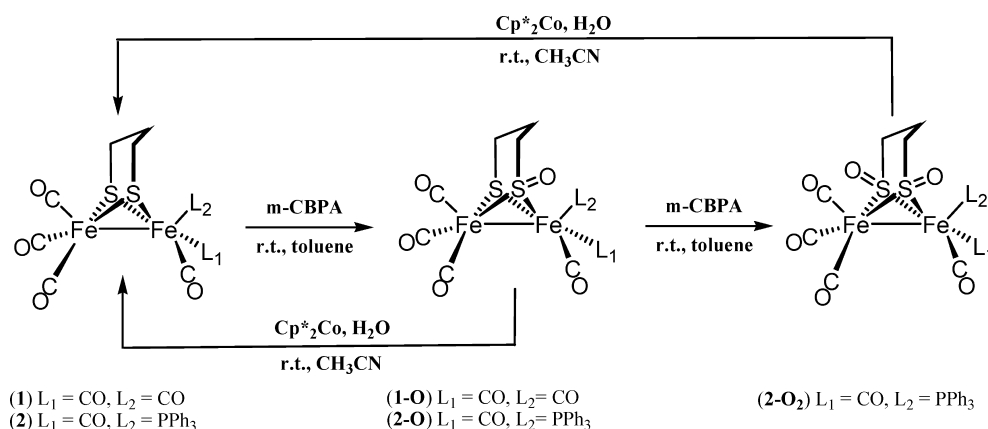
complex **4**, $(\mu\text{-pdt})[\text{Fe}(\text{CO})_2\text{PMe}_3]_2$, for which the stabilizing effect of better donors was expected to be more likely to form metal-based $\text{Fe}^{\text{II}}(\mu\text{-O})\text{Fe}^{\text{II}}$ species as suggested by the above DFT investigation. Complex **4** rapidly reacts with O_2 to generate a dark, insoluble residue. Unlike complexes **1** and **2**, complex **4** vigorously reacts with H_2O_2 in acetone at 22 °C to form light orange precipitates with gas evolution (assumed to be CO or CO_2). The orange non-CO-containing product is only slightly soluble in water and remains uncharacterized. When oxygenation of **4** with *m*-CPBA was performed following the procedure as for **1** and **2**, a small amount of product, $(\mu\text{-pst})[\text{Fe}(\text{CO})_2\text{PMe}_3]_2$ (**4-O**), was slowly formed while most of the starting material decomposed (see Scheme 3). The final yield of **4-O** was ca. 8%. Another trace byproduct characterized by higher CO stretching frequencies (2033 and 1981 cm^{-1}) was also detected. This species was isolated by co-crystallization with **4-O** in hexane solution. X-ray diffraction analysis revealed that the byproduct is a mono iron(II) dicarboxylate dicarbonyl, $\text{Fe}(\text{CO})_2(\text{PMe}_3)_2(m\text{-Cl-PhCOO}^-)_2$, **6** (see Scheme 3 and Figure S3f, Supporting Information). This product implicates at least some Fe-based oxidation.

In order to probe the effect of Fe oxidation state on the oxygenation of diiron complexes, complex **5**, a $\text{Fe}^{\text{II}}\text{Fe}^{\text{II}}$ species, was exposed to *m*-CPBA (Scheme 4). At 22 °C, in CH_2Cl_2 , quantitative conversion to its S-oxygenate was observed. The **5-O** complex is stable to excess *m*-CPBA, as no additional oxygenated species was observed.

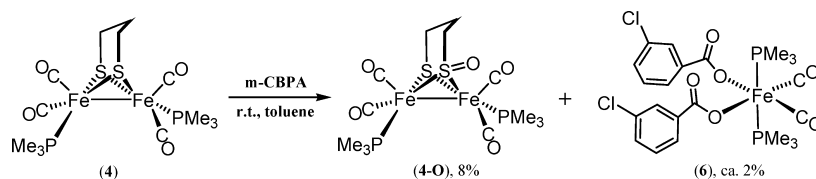
During attempts to deoxygenate **1-O** by phosphines, an alternate route to complexes **2-O** and **4-O** was discovered, Scheme 5. Pursuing this synthetic approach, we noticed that ligand substitution of **1-O** required harsher conditions than with **1**. For example, complex **1-O** does not show obvious reactivity with PMe_3 in hexane at 22 °C and only slowly forms the mono- PMe_3 -substituted product, $(\mu\text{-pst})[\text{Fe}(\text{CO})_3][\text{Fe}(\text{CO})_2\text{PMe}_3]$ (**3-O**) at 68 °C. In refluxing toluene (110 °C), complex **4-O** was prepared from complex **1-O** and excess PMe_3 by the ligand exchange process. In contrast, **1** readily reacts with PMe_3 in hexane at 22 °C to generate mono- PMe_3 -substituted product, $(\mu\text{-pdt})[\text{Fe}(\text{CO})_3][\text{Fe}(\text{CO})_2\text{PMe}_3]$ (**3**), and disubstitution by PMe_3 occurs at 68 °C. For comparison, the rates of CO/ PMe_3 exchange reactions of **1** and **1-O** in toluene were investigated under similar pseudo-first-order conditions for **1** and **1-O** using 20 equiv of PMe_3 . Through monitoring the disappearance of the $\nu(\text{CO})$ IR band at 2076(m) for **1** at 22 °C, the observed pseudo-first-order rate constant is found to be $1.47 \times 10^{-4} \text{ s}^{-1}$, while the exchange reaction for **1-O** is immeasurably slow. At 90 °C, the observed rate constant for **1-O**/ PMe_3 is $4.2 \times 10^{-5} \text{ s}^{-1}$ (disappearance of $\nu(\text{CO})$, 2083(m)). Detailed kinetic studies will be reported in a separate publication.

The IR spectra in the CO stretching region of all sulfur-oxygenated complexes are displayed in Figure S1 (Supporting Information), and IR data including reference complexes are compared in Table 1. Complex **1-O** features a $\nu(\text{CO})$ IR absorption pattern similar to that of complex **1** with $\nu(\text{CO})$ values shifted ca. 10 cm^{-1} higher than for complex **1**, indicative of the poorer donating ability of propanesulfonato thiolate ($-\text{S}(\text{CH}_2)_3\text{S}(\text{O})-$) compared to propanedithiolate ($-\text{S}(\text{CH}_2)_3\text{S}-$). Similarly, the $\nu(\text{CO})$ order in the series of **2** < **2-O** < **2-O₂** corresponds to decreasing donating strength of bidentate bridging ligands of $-\text{S}(\text{CH}_2)_3\text{S}-$, $-\text{S}(\text{CH}_2)_3\text{S}(\text{O})-$, and $-(\text{O})\text{S}(\text{CH}_2)_3\text{S}(\text{O})-$. Similar trends can be also deduced from comparison of **4** and **4-O**, and of **5** and **5-O**. The byproduct, **6**, isolated from the oxygenation of **4**, exhibits two

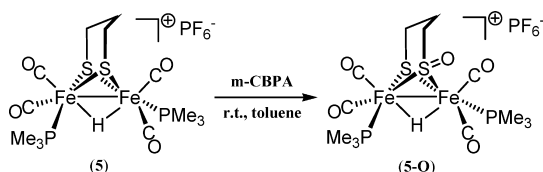
Scheme 2



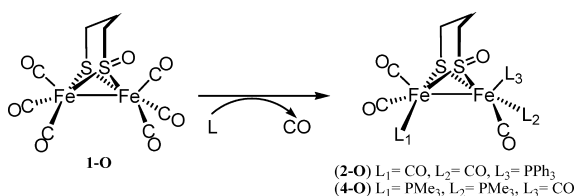
Scheme 3



Scheme 4



Scheme 5



strong CO absorptions at 2033(s) and 1981(s), consistent with the vibrational modes of a *cis*-dicarbonyl species.

Electrochemical Studies of 1-O, 2-O, 2-O₂, and 4-O. The redox properties of sulfur-oxygenated complexes were studied by cyclic and differential pulse voltammetry. The electrochemical data are given in Table 3. According to previous reports, the first reduction event is assigned to Fe(I)Fe(I)/Fe(I)Fe(0).^{51,52} The oxidative features may relate to a Fe(I)Fe(II)/Fe(I)Fe(I) process; however, S-based oxidation is also possible. Figure 4 presents the CV and DPV curves of 1-O. Recorded CV and DPV curves for 2-O, 2-O₂, and 4-O are in the Supporting Information (Figure S2). In comparison to their non-oxygenated analogues, S-oxygenates exhibit redox couples at more positive potentials, consistent with the electron-withdrawing ability of $-(\text{O})\text{S}(\text{CH}_2)_3\text{S}(\text{O})-$ and $-(\text{O})\text{S}(\text{CH}_2)_3\text{S}-$ as inferred from IR studies.

In addition to the redox event at -1.58 V, complex 1-O displays a second redox event at -1.70 V, as shown in Figure

Table 3. Cyclic Voltammetry Data versus Fc^{+/0} for the Sulfur-Oxygenated Complexes (1-O, 2-O, 2-O₂, and 4-O) and Reference Complexes in CH₃CN Electrolyte (0.1 mM Bu₄N⁺BF₄⁻; Scan Rate, 100 mV/s)

complex	oxidation	Fe(I)Fe(II)/ Fe(I)Fe(I)	Fe(I)Fe(I)/ Fe(I)Fe(0)	further reduction
1	—	0.82	-1.70	-2.32
2	0.66	0.27	-1.87	-2.24
4	0.65, 0.23	-0.14	-2.37	—
1-O	—	0.95	-1.58	-1.70, -2.25
2-O	—	0.48	-1.77	-1.97, -2.3
2-O ₂	—	0.65	-1.72	-1.98
4-O	0.67	0.03	-2.21	-2.38

4. The latter reduction potential is identical to that of the Fe(I)Fe(I)/Fe(I)Fe(0) couple of complex 1. According to the DPV studies, the extracted Faradaic current intensity of the first reduction of 1-O is dominant over that of the second reduction. A similar phenomenon is seen for complex 4-O. The second reduction at -2.38 V of 4-O is 170 mV more negative than its first reduction and lies at almost the same position as the first reduction of complex 4. Complex 2-O displays two additional reduction events at -1.97 and -2.3 V, ca. 200 mV more negative than its Fe(I)Fe(I)/Fe(I)Fe(0) couple. For complex 2-O₂, only one additional reduction event at -1.98 V was observed. The most reasonable explanation for these results is that some

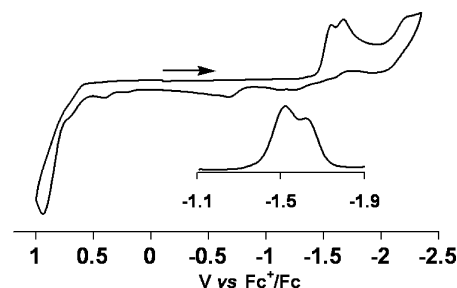


Figure 4. CV and DPV (inset) curves of the sulfur-oxygenated complex 1-O in CH₃CN. All potentials are referenced vs Fc^{+/0} (scan rate = 100 mV/s, 0.1 M [Bu₄N]⁺[BF₄]⁻, 22 °C).

(51) Chong, D. S.; Georgakaki, I. P.; Mejia-Rodriguez, R.; Samabria-Chinchilla, J.; Soriaga, M. P.; Darensbourg, M. Y. *Dalton Trans.* **2003**, 4158–4163.

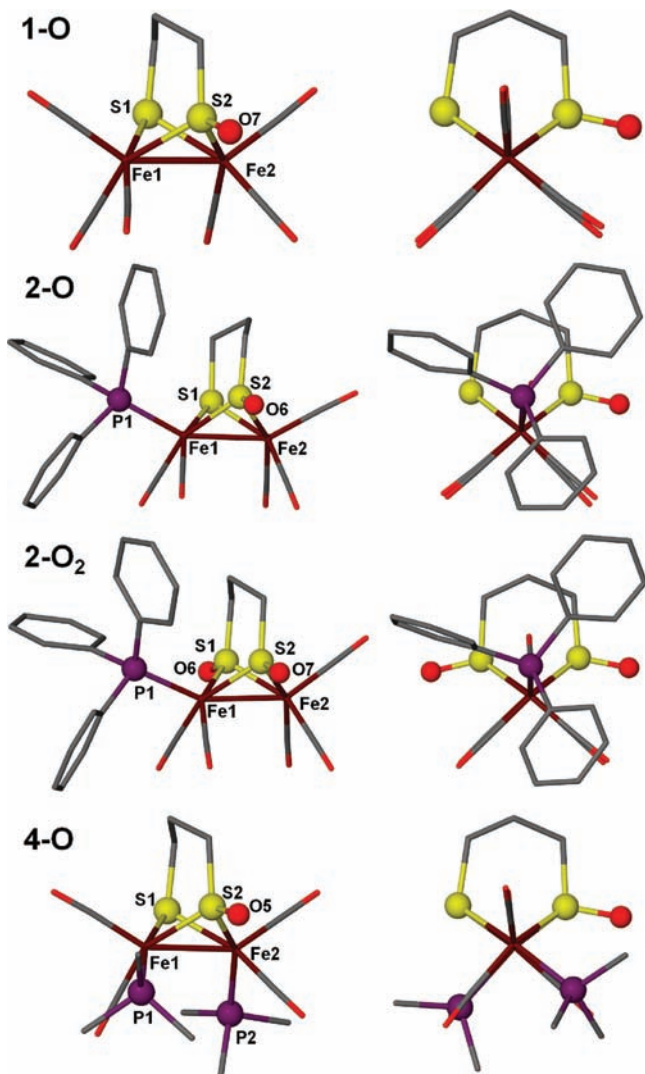


Figure 5. Molecular structures of the sulfur-oxygenated complexes (**1-O**, **2-O**, **2-O₂**, and **4-O**) given in two perspectives, perpendicular to and along the Fe–Fe bond vector. For **2-O** and **2-O₂**, the PPh₃ ligand is in the front.

reductive deoxygenation process produces the precursor dithiolate *in situ*. Countering this argument is the fact that repeated scans did not change the relative intensities of the two reduction events in any of the oxygenates.

Molecular Structures of Oxygenated Species (1-O, 2-O, 2-O₂, and 4-O). The molecular structures of these complexes verified S-oxygenation, Figure 5. Selected metric data are listed in Table 4. All structures adopt the well-known butterfly Fe₂S₂ core geometry with Fe–Fe distances in the 5.6 Å range, slightly longer than their non-oxygenated counterparts.^{19,30,53} The Fe–Fe distance of complex **4-O** is even longer by ca. 0.094 Å than that of {(μ-pdt)(μ-H)[Fe(CO)₂PM₃]₂}⁺PF₆[−] (2.578 Å).¹⁹ The S–O vector in each is roughly perpendicular to the Fe–Fe vector. The PPh₃ ligands of complexes **2-O** and **2-O₂** occupy apical positions, which is the same as the reported structure of complex **2**. The PMe₃ ligands of complex **4-O** are both at basal

Table 4. Selected Metric Data for the Sulfur-Oxygenated Complexes (**1-O**, **2-O**, **2-O₂**, and **4-O**)

	1-O	2-O	2-O₂	4-O
Fe1–Fe2 (Å) ^a	2.5765(8) (2.5103(11))	2.5583(16) (2.5247(6))	2.5783(13) (2.5247(6))	2.6173(12) (2.555(2))
Fe1–S1 (Å)	2.2563(12)	2.22(2)		2.2794(13)
Fe1–S1(=O) (Å)			2.1840(17)	
Fe1–S2(=O) (Å)	2.1654(12)	2.219(2)	2.1906(16)	2.1650(17)
S2=O (Å)	1.495(2)	1.405(7)	1.487(4)	1.5168(19)
Fe–P1 (Å)		2.228(2)	2.2312(17)	2.2133(17)
S1–Fe1–S2 (deg)	82.40(4)	81.21(7)	80.63(6)	81.65(6)
Fe1–S2–Fe2 (deg)	73.04(4)	70.41(7)	72.18(5)	74.36(5)

^aThe values in parentheses are the Fe–Fe distance of parent non-oxygenates.

sites. One molecule of water binds with two molecules of **4-O** via hydrogen-bonding interactions (see Figure S3e, Supporting Information). The hydrogen bond defined by O···O distance between S=O and H₂O is 2.899 Å (the calculated distance of OH···OS is 2.030 Å).

For the mono-oxy complexes **1-O**, **2-O**, and **4-O**, the Fe–S(O) distance is shorter than the corresponding Fe–S distance while the bis-oxy complex, **2-O₂**, possesses identical, short Fe–S distances. The S–O distance of complex **1-O** is 1.495 Å, ca. 0.09 Å longer than that of **2-O** (1.405 Å). Further oxygenation of **2-O** led to longer S–O distances in **2-O₂**, symmetry generated identical at 1.487 Å. Complex **4-O** exhibits the longest S–O distance of the series. This result is explained by the S–O bond polarization from H-bonding to water (*vide supra*). While these comparisons suggest a small influence of the S-attached O atom on the core structure of diiron dithiolates, there is no apparent trend in the S=O distances with electron-richness of the diiron complex.

CO Site-Exchange Processes of Complex 1-O and Variable-Temperature ¹³C NMR Studies. A fundamental property of the (μ-SRS)[Fe(CO)₃]₂ molecule is the intramolecular site exchange which takes place on each Fe(CO)₃ unit, interchanging apical and basal CO groups.^{29,54,55} The barrier to this rotation is affected by substituent ligands.^{29,54,55} Hence, the S-oxygenates provide an opportunity to investigate the effect of S-modification in the bridging propane dithiolate linker on the CO intramolecular exchange processes in (μ-SRS)[Fe(CO)₃]₂ vs (μ-SRSO)[Fe(CO)₃]₂ complexes.

Variable-temperature ¹³C NMR spectra of **1-O**, recorded on a 500 MHz NMR spectrometer in the temperature region of 30 to −60 °C, are displayed in Figure 6 (Figure S5 in the Supporting Information contains spectra for **1** recorded under identical conditions). At 20 °C, **1-O** displays a broad resonance at δ = 207.8 ppm which is assigned to the six rapidly exchanging CO ligands. With increase of the temperature to 30 °C, the signal sharpens, while upon cooling the sample the resonance broadens, with coalescence occurring at −10 °C. Below −10 °C, the signal begins to split into separate signals, and by −40 °C, complete resolution into three single resonances is observed, with chemical shifts at δ = 207.8, 207.4, and 207.0 ppm and in a ratio of approximately 1:1:1. As the broadening resulting from decreased motion of the S-to-S linker should affect the signals corresponding to the basal COs approximately the same, the fact that the resonance at 207.4 ppm changes rapidly upon cooling further indicates that it should correspond

(52) Capon, J. F.; Ezzaher, S.; Gloaguen, F.; Petillon, F. Y.; Schollhammer, P.; Talarmin, J.; Davin, T. J.; McGrady, J. E.; Muir, K. W. *New J. Chem.* **2007**, *31*, 2052–2064.
 (53) Lyon, E. J.; Georgakaki, I. P.; Reibenspies, J. H.; Darensbourg, M. Y. *Angew. Chem., Int. Ed.* **1999**, *38*, 3178–3180.

(54) Singleton, M. L.; Jenkins, R. M.; Klemashevich, C. L.; Darensbourg, M. Y. *C. R. Chim.* **2008**, *11*, 861–874.
 (55) Tye, J. W.; Darensbourg, M. Y.; Hall, M. B. *Inorg. Chem.* **2006**, *45*, 1552–1559.

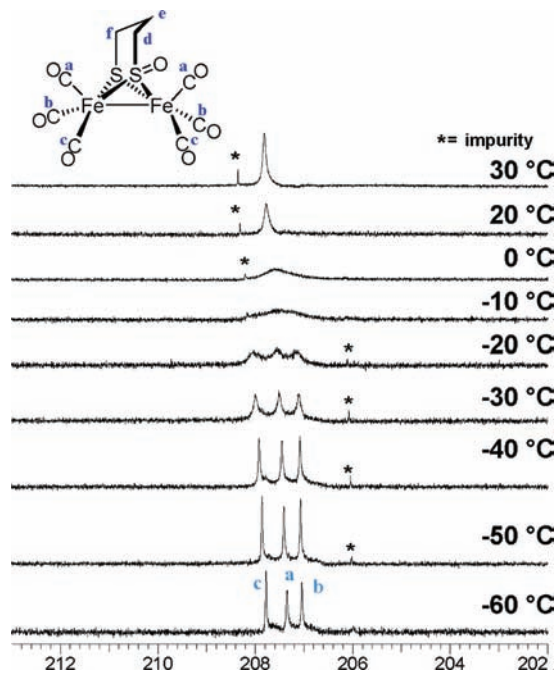


Figure 6. Variable-temperature ^{13}C NMR studies of complex **1-O** from -60 to 30 $^{\circ}\text{C}$ (CD_2Cl_2 solution, in CO region); signals indicated with an asterisk are unknown impurities.

to the apical CO. The assignments of the resonances at 207.8 and 207.0 ppm can be made by comparison of this complex to previously reported diiron models where CO has been substituted by a better donor ligand.^{29,54} In the spectra of these complexes, all CO signals show a marked downfield shift likely resulting from increased π -backbonding. Since the COs trans to the sulfenato should experience a smaller amount of backbonding than the COs trans to the thiolate, the resonance at 207.0 ppm is assigned to the former and the remaining resonance at 207.8 ppm to the latter.

Ideally, six COs should be characterized by individual signals when the bridge flip of $-\text{S}(\text{CH}_2)_3\text{S}(\text{O})-$ is stopped; however, this was not observed for the temperature range explored in this study. From the exchange rate constant at coalescence ΔG^\ddagger is estimated as 45 kJ/mol (or 10.7 kcal/mol); the full line shape analysis found a similar value of $\Delta G^\ddagger = 48$ kJ/mol (or 11.4 kcal/mol). See Figure S4 (Supporting Information) for the Eyring plots used to derive ΔG^\ddagger and ΔH^\ddagger for the CO rotation process.

Under experimental conditions similar to those used for **1-O**, the spectra for complex **1** were recorded over a larger temperature range than previously reported.²⁹ Based on the new spectra, the coalescence temperature was observed at -50 $^{\circ}\text{C}$ for complex **1**, which is about 40 $^{\circ}\text{C}$ lower than that of complex **1-O**, and the peak separation between apical and basal signals was greater than twice that observed for **1-O** (see Figure S5, Supporting Information). Both of these facts indicate that the $\text{Fe}(\text{CO})_3$ unit of complex **1** is more mobile than that of complex **1-O**. In fact, the ΔG^\ddagger from the exchange rate constant at coalescence for complex **1** was estimated to be 36 kJ/mol (or 8.6 kcal/mol), which is ~ 10 kJ/mol less than that of the sulfenato derivative. This difference indicates that modification of the thiolate S into a sulfenato increases the barrier for CO site exchange on the all-CO complex.

Computational (DFT) Results. While DFT computations that defined the transition-state structure resulting from the intramolecular interchange of apical and basal CO groups in complex

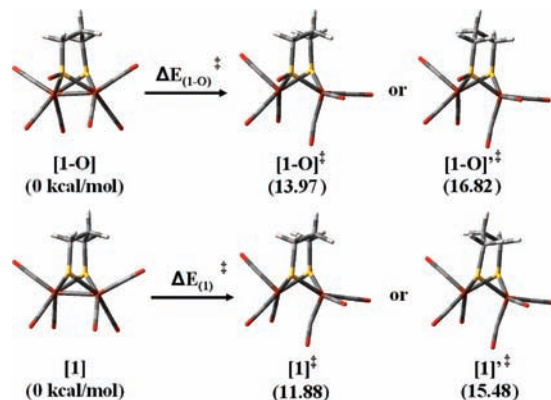


Figure 7. Ground-state and transition-state structures of **1-O** (top) and **1** (bottom) with corresponding energies given in kcal/mol obtained by DFT computations (B3LTP/D95&LANL2DZ) for one $\text{Fe}(\text{CO})_3$ unit rotation.

1 were earlier reported,^{29,55} the structure has been reexamined in order to compare results under the same computational settings as used for complex **1-O**. Figure 7 (top) displays the geometry-optimized ground-state structure, **[1-O]**, of complex **1-O**, along with two transition states, **[1-O][‡]** and **[1-O][‡]**, calculated for the CO site-exchange process of one $\text{Fe}(\text{CO})_3$ unit. The latter differs in the orientation of the bridgehead carbon in the S-to-S linker. Note that the $\text{Fe}(\text{CO})_3$ unit experiencing rotation inverts its square pyramidal geometry with the inverted apical CO lying under the Fe–Fe vector at a semibringing position, similar to what is observed for mixed-valent $\text{Fe}^{\text{I}}\text{Fe}^{\text{II}}$ species.^{56–59} The total energy difference between the ground state and the transition state is 13.97 kcal/mol calculated at the level of B3LTP/D95&LANL2DZ. In Figure 7 (bottom) is given the ground-state structure and the transition-state structures of **1** along one $\text{Fe}(\text{CO})_3$ rotation. The energy barrier required for such site-exchange is 11.88 kcal/mol.⁵⁵ The DFT results find that the CO site-exchange process is more accessible for **1** than for **1-O** since $\Delta E_{(1-O)}^\ddagger$ is smaller than $\Delta E_{(1)}^\ddagger$ by both calculations. The bridging S–S linker flip would disfavor the CO site-exchange process by ca. 3 kcal/mol for both **1** and **1-O**. For instance, isomer **[1][‡]** is 2.85 or 2.69 kcal/mol more stable than the bridge-flipped isomer, **[1][‡]**. Calculations of both complexes at the level of B3LTP/cc-PVDZ&LANL2DZ yield similar results (see Figure S6, Supporting Information). Qualitatively these theoretical results are acceptable, although in both cases the calculated values are higher than the experimental values of 10.07 kcal/mol for **1-O** and 8.6 kcal/mol for **1**.

Chemical and Electrochemical Deoxygenation Studies. Deoxygenation of the sulfur-oxygenated complexes is of particular importance as it might be related to the reductive reactivation mode of the active site of aerobically isolated $[\text{FeFe}]\text{-H}_2\text{ase}$.² In addition, deoxygenation with suitable oxygen-transfer reagents could indicate relative S=O bond energies in such complexes.⁶⁰ We have attempted to use phosphines as O-atom acceptors; however, as discussed above, with PPh_3 and PMe_3 , only phosphine-substituted diiron complexes were identified as

(56) Liu, T.; Darensbourg, M. Y. *J. Am. Chem. Soc.* **2007**, *129*, 7008–7009.

(57) Thomas, C. M.; Liu, T.; Hall, M. B.; Darensbourg, M. Y. *Inorg. Chem.* **2008**, *47*, 7009–7024.

(58) Justice, A. K.; Rauchfuss, T. B.; Wilson, S. R. *Angew. Chem., Int. Ed.* **2007**, *46*, 6152–6154.

(59) Justice, A. K.; De Gioia, L.; Nilges, M. J.; Rauchfuss, T. B.; Wilson, S. R.; Zampella, G. *Inorg. Chem.* **2008**, *47*, 7405–7414.

(60) Holm, R. H.; Donahue, J. P. *Polyhedron* **1993**, *12*, 571–589.

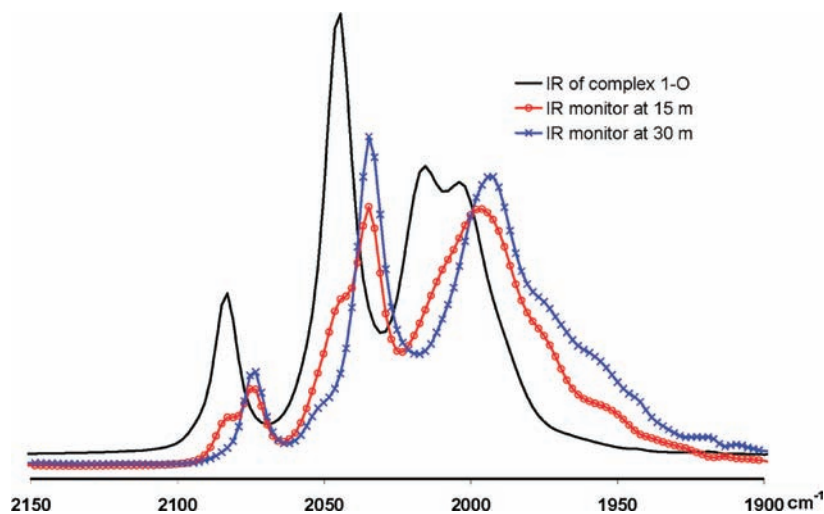


Figure 8. IR monitor of deoxygenation of **1-O** with Cp^*_2Co in CH_3CN in the presence of H_2O (2% V/V).

products. In the presence of the bulky (*t*-Bu) $_3\text{P}$, which did not demonstrate CO substitution with complex **1**, complex **1-O** remained intact under various reaction conditions. Whether the lack of O-atom transfer to phosphines is a reflection of poor kinetics or the actual thermodynamic preference is, at this stage, unclear as examples of very slow rates of uncatalyzed O-atom-transfer reactions are well known.⁶⁰

Reductive deoxygenation of **1-O** was examined using Cp^*_2Co (ca. -1.9 V vs Fc^+/Fc) as reductant. In the presence of $\text{CH}_3\text{CN}:\text{H}_2\text{O}$ (50:1, V/V), complex **1-O** was reduced by 2 equiv of Cp^*_2Co , resulting in the formation of complex **1** over the course of 30 min in an isolated yield of 50% (see Scheme 2 and Figure 8). Replacement of CH_3CN by THF gave the same results. However, the use of anhydrous CH_3COOH and CF_3COOH as proton source was not effective as both directly react with the Cp^*_2Co reductant. In the absence of H_2O , complex **1-O** was reduced by Cp^*_2Co in CH_3CN to an unknown air-sensitive species with multiple CO stretches, a species that was not observed in the presence of H_2O . Subsequent treatment of the *in situ* generated complex with H_2O slowly led to the formation of complex **1** in low yield.

By following the deoxygenation procedure used for complex **1-O**, complexes **2-O** and **2-O₂** were transformed to complex **2** with 2 and 4 equiv of Cp^*_2Co , respectively, in ca. 10% yield. Unknown CO-containing species were detected by IR in the deoxygenation processes of both complex **2-O** and **2-O₂**.

Complexes **3-O** and **5-O** were also examined for deoxygenation in the same manner. Deoxygenation of **5-O** was complicated by concurrent reductive deprotonation. The $\nu(\text{CO})$ IR monitor indicated that a small amount of complex **5** was reclaimed from **5-O**, while complex **4-O** was also generated via proton loss from the bridging hydride. Complex **4-O** was not reduced by Cp^*_2Co in the absence or presence of H_2O .

Alternatively, electrochemical methods were used to control the reduction potential for deoxygenation of complex **4-O**. In $\text{CH}_3\text{CN}:\text{H}_2\text{O}$ (50:1, V/V), cathodic bulk electrolysis was set at 2.3 V vs Fc^+/Fc , which is about 100 mV more negative than the $\text{Fe}^{\text{I}}\text{Fe}^{\text{I}}/\text{Fe}^{\text{I}}\text{Fe}^0$ couple of complex **4-O**. In Figure 9 (top), curve A represents the CV of **4-O**, and in Figure 9 (bottom), the red line (IR A) displays the IR spectrum of **4-O**. After a total charge of 0.43 Q (ca. 1 equiv of electrons) was passed at the controlled potential, the second CV, which is plotted as curve B, was recorded. In the CV labeled as B, the current intensity of the

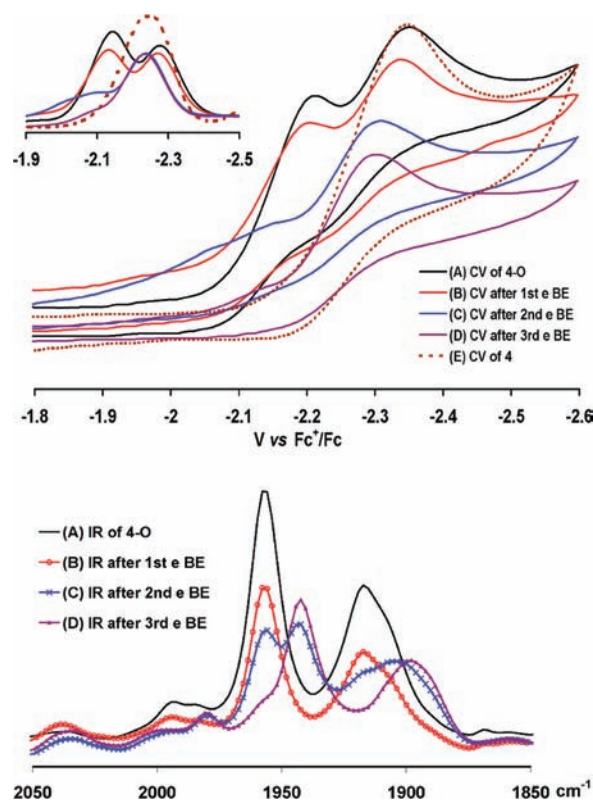


Figure 9. CV (top), DPV (top, inset), and IR measurements (bottom) of deoxygenation studies of **4-O** via bulk electrolysis.

first reduction diminished while the second peak intensified and shifted anodically. At this point a sample was taken from the electrochemical cell and its IR spectrum recorded. A decrease in $\nu(\text{CO})$ IR intensities indicated consumption of **1-O** during bulk electrolysis, although no new species was identified. When the second equivalent of electrons was supplied, the difference of the current intensity between the first and the second reduction waves was further noticeable. The IR spectrum (IR B) taken subsequently suggests the formation of complex **4** with its characteristic band at 1942 cm^{-1} and the presence of remaining complex **4-O**. The first reduction peak completely disappeared in the third CV (CV C), which was measured after the third equivalent of electrons was passed through the working

electrode. The observed reduction at -2.35 V shifted ca. 30 mV anodically in comparison to the original second reduction. The corresponding IR (D) exhibited CO stretches exclusively for complex **4**. The yield of complex **4** from this approach was estimated to be ca. 25% based on the relative CO stretch intensity of **4-O** and **4**.

The bulk electrolysis was also monitored by the DPV mode of analysis (inset in Figure 9, top), which more clearly displays the changes of the reduction events during the stepwise bulk electrolysis. To further verify the efficiency of the electrochemical approach, deoxygenation by bulk electrolysis was applied to complex **1-O**. Under the same experimental conditions, the electrochemical deoxygenation of complex **1-O**, which was monitored by CV, DPV, and IR *in situ* (see Figure S7, Supporting Information), was shown to take up 2 equiv of electrons, similar to its chemical reduction and deoxygenation.

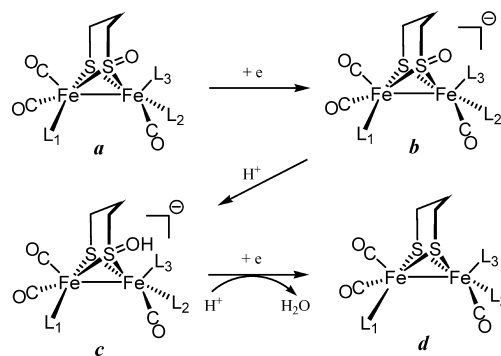
Conclusions and Comments

Oxygenates and Deoxygenation. The diiron complexes with S-oxygenated bridging ligands demonstrates good stability and physical properties similar to those of the parent dithiolates that have served to provide insight into the unique diiron subsite of [FeFe]-H₂ase. Electronic modulation of (μ -pdt)[Fe(CO)₃]₂ via CO/L exchange influences the O-atom uptake from *m*-CPBA of the parent diiron dithiolates. The less electron rich complexes allowed isolation of the kinetically controlled S-oxygenate products. The more electron rich complexes led to decomposition, presumably from the thermodynamic (DFT-predicted) Fe-based oxygenation. As Fe^{II} complexes have weak Fe–CO bonds, the decomposition is to be expected. The isolation of monoiron(II) complex **6** is evidence of such Fe-based reactivity; however, whether the oxidation is inner sphere or outer sphere is not known.

Sulfur-oxygenation presents an additional way to influence the fundamental properties of the versatile (μ -SRS)[Fe(CO)₃]₂ complex. Sensitivity to CO substitution,^{30,61,62} redox levels,⁶³ the nature of R,⁶⁴ and S/Se or P exchange^{65–67} is now augmented by sulfur oxygenation. While still a good bidentate bridging ligand, the sulfenato moiety is a poorer electron donor, reducing electron density at iron and resulting in slower rates of ligand substitution and greater barriers to intramolecular CO site exchange.

Reductive deoxygenation was observed by both electrochemical and bulk chemical reduction. In both cases water served as an optimal proton source, presumably following the mechanism described in Scheme 6 as a proton-coupled electron-transfer (PCET) process. The sequence proposes an initial one-electron reduction of **a**, the neutral sulfur-

Scheme 6



oxygenated species, to form anion **b** via an electron-transfer (ET) process. The first step cannot be protonation at O of S=O because protonation should lead to changes in $\nu(\text{CO})$ values which are not observed in the presence of H₂O, CH₃COOH, or CF₃COOH as proton sources. The ET step is followed by or concurrent with a proton-transfer (PT) process to form species **c** shown in Scheme 6, since the second electron reduction is not accessible by the reducing ability of Cp*₂Co in the presence of H₂O or at the reduction potential applied in the bulk electrolysis. Subsequently, the second ET and the second PT will take place to give the deoxygenated product **d**. More likely, the second ET will occur first because the second PT is relatively difficult while the first PT should make the second ET favorable. The nature of the deoxygenation of the Fe^{II}Fe^I complex **5-O** should follow the same mechanism as for the Fe^{II}Fe^I S-oxygenated complexes. A definite conclusion to be taken from the deoxygenation studies is as follows: *sulfur deoxygenation is a two-electron process*.

Biological Relevance of Oxygenation and Deoxygenation Studies. Using protein film electrodes, Armstrong et al.² explored the air sensitivity of [FeFe]-H₂ase from *D. desulfuricans* at the H_{ox} (Fe^{II}Fe^I) and the anaerobically, electrochemically oxidized state (242 mV vs SHE). As was found for the Fe^{II}Fe^I mixed-valent model complexes,^{56–59} the H_{ox} state is highly air sensitive, resulting in permanent irreversible damage/degradation, most likely due to the promotion of O₂ reactivity by the radical character of Fe^{II}Fe^I. We have found that the Fe^{II}Fe^{II} complex **5** is air stable and, when forced by strong O-donor agents, the O-atom uptake that occurs at sulfur can be reversed under reducing conditions. Armstrong's anaerobically overoxidized [FeFe]-H₂ase enzyme,² presumed to be at the Fe^{II}Fe^{II} redox level, is said to be "protected" from permanent O₂ damage in that activity can be partially regained when the potential is swept or stepped to more negative values. As the electronic structure of this anaerobically oxidized *Dd* [FeFe]-H₂ase state is likely to be the same as that of the Fe^{II}Fe^{II} in complex **5**, and as S-oxygenation is known for complex **5**, we posit that a similar process may occur in the fully oxidized state of the enzyme and that reductive repair can remove S-based oxygenation as we have seen for complex **5**.

A final point is that S-oxygenation of complex **5** requires a peroxy species rather than molecular O₂. Whether such reactive oxygen species, such as OOH⁻, can be generated in the metalloprotein environment is to our knowledge unknown and cannot be excluded as unreasonable. A simple point is clear: *if oxygen exposure of the enzyme active site results in sulfur oxygenation, then such oxygen "damage" can be reductively repaired*.

- (61) Gao, W. M.; Ekstrom, J.; Liu, J. H.; Chen, C. N.; Eriksson, L.; Weng, L. H.; Akermark, B.; Sun, L. H. *Inorg. Chem.* **2007**, *46*, 1981–1991.
 (62) Justice, A. K.; Zampella, G.; De Gioia, L.; Rauchfuss, T. B.; van der Vlugt, J. I.; Wilson, S. R. *Inorg. Chem.* **2007**, *46*, 1655–1664.
 (63) Borg, S. J.; Behrsing, T.; Best, S. P.; Razavet, M.; Liu, X. M.; Pickett, C. J. *J. Am. Chem. Soc.* **2004**, *126*, 16988–16999.
 (64) Seyferth, D.; Womack, G. G.; Song, L. C. *Organometallics* **1983**, *2*, 776–779.
 (65) (a) Seyferth, D.; Henderson, R. S. *J. Organomet. Chem.* **1980**, *204*, 333–343. (b) Seyferth, D.; Brewer, K. S.; Wood, T. G.; Cowie, M.; Hiltz, R. W. *Organometallics* **1992**, *11*, 2570–2579.
 (66) Gao, S.; Fan, J. L.; Sun, S.; Peng, X. J.; Zhao, X.; Hou, J. *Dalton Trans.* **2008**, 2128–2135.
 (67) Harb, M. K.; Niksch, T.; Windhager, J.; Görls, H.; Holze, R.; Lockett, L. T.; Okumura, N.; Evans, D. H.; Glass, R. S.; Lichtenberger, D. L.; El-khateeb, M.; Weigand, W. *Organometallics* **2009**, *28*, 1039–1048.

Acknowledgment. We acknowledge financial support from the National Science Foundation (CHE-0616695) with contributions from the R.A Welch Foundation (A-0924) and The China Scholarship Council for support for B.L.

Supporting Information Available: Full structure files, in CIF format, of complexes **1-O**, **2-O**, **2-O₂**, **4-O**, and **6**; IR spectra of sulfur oxygenated complexes **1-O**, **2-O**, **2-O₂**, **4-O**, **5-O**, and **6**; CV and DPV of **2-O**, **2-O₂**, and **4-O**; CV, DPV, and IR studies of deoxygenation of **1-O** via bulk electrolysis; thermal ellipsoid representations of **1-O**, **2-O**, **2-O₂**, **4-O** and **6**; linear

Eyring plots of **1-O** to derive ΔG^\ddagger and ΔH^\ddagger for intramolecular CO exchange; VT ¹³CNMR of complex **1**; DFT optimized structures of **1-O**, **2-O**, **2-O₂**, **4-O**, and **5-O** with corresponding frontier orbitals as well as structural parameters compared with experimental values; full DFT results about total energy comparison of sulfur-oxygenates and corresponding μ -oxo species; and complete ref 41. This material is available free of charge via the Internet at <http://pubs.acs.org>.

JA9016528